

# The effect of solvent quality on pathway-dependent solution-state self-assembly of an amphiphilic diblock copolymer

Cite as: J. Appl. Phys. **127**, 125104 (2020); <https://doi.org/10.1063/1.5139230>

Submitted: 19 November 2019 . Accepted: 07 March 2020 . Published Online: 23 March 2020

Shrinivas Venkataraman, Guangmin Wei, Kenneth P. Mineart, James L. Hedrick, Vivek M. Prabhu , and Yi Yan Yang



[View Online](#)



[Export Citation](#)



[CrossMark](#)

Lock-in Amplifiers  
Find out more today



 Zurich  
Instruments

# The effect of solvent quality on pathway-dependent solution-state self-assembly of an amphiphilic diblock copolymer

Cite as: J. Appl. Phys. 127, 125104 (2020); doi: 10.1063/1.5139230

Submitted: 19 November 2019 · Accepted: 7 March 2020 ·

Published Online: 23 March 2020



View Online



Export Citation



CrossMark

Shrinivas Venkataraman,<sup>1,a),b)</sup> Guangmin Wei,<sup>2,c)</sup> Kenneth P. Mineart,<sup>2,d)</sup> James L. Hedrick,<sup>3</sup> Vivek M. Prabhu,<sup>2,b)</sup>  and Yi Yan Yang<sup>1,b)</sup>

## AFFILIATIONS

<sup>1</sup>Institute of Bioengineering and Nanotechnology, 31 Biopolis Way, The Nanos, Singapore 138669

<sup>2</sup>Material Measurement Laboratory, National Institute of Standards and Technology, 100 Bureau Drive, Gaithersburg, Maryland 20899, USA

<sup>3</sup>IBM Almaden Research Center, 650 Harry Road, San Jose, California 95120, USA

**Note:** This paper is part of the Special Topic on Polymer-Grafted Nanoparticles.

**a)** **Current address:** ACM Biolabs Pte. Ltd., 71 Nanyang Drive, NTU Innovation Centre, #2M-02, Singapore 638075.

**b)** **Authors to whom correspondence should be addressed:** [svenkataraman@acmbiolabs.com](mailto:svenkataraman@acmbiolabs.com); [vprabhu@nist.gov](mailto:vprabhu@nist.gov); and [yyyang@ibn.a-star.edu.sg](mailto:yyyang@ibn.a-star.edu.sg)

**c)** **Current address:** School of Chemical and Biomedical Engineering, Nanyang Technological University, 62 Nanyang Drive, Singapore 637459.

**d)** **Current address:** Department of Chemical Engineering, Bucknell University, Lewisburg, Pennsylvania 17837, USA.

## ABSTRACT

The cholesterol-functionalized polycarbonate-based diblock copolymer, PEG<sub>113</sub>-*b*-P(MTC-Chol)<sub>30</sub>, forms pathway-dependent nanostructures via dialysis-based solvent exchange. The initial organic solvent that dissolves or disperses the polymer dictates a self-assembly pathway. Depending upon the initial solvent, nanostructures of disk-like micelles, exhibiting asymmetric growth and hierarchical features, are accessible from a single amphiphilic precursor. Dioxane and tetrahydrofuran (THF) molecularly dissolve the block copolymer, but THF yields disks, while dioxane yields stacked disks after dialysis against water. Dimethylformamide and methanol display dispersed disks and then form stacked disk structures after dialysis. The path-dependent morphology was correlated to solubility parameters, an understanding of which offers routes to tailor self-assemblies with limited sets of building blocks.

<https://doi.org/10.1063/1.5139230>

## INTRODUCTION

Spontaneous self-assembly of amphiphilic block copolymers in a block-selective solvent enables nanostructures such as spherical micelles, cylindrical micelles, and bilayers.<sup>1</sup> Through molecular design of the functional groups, further association of these precursor structures can produce pathway-dependent hierarchical or supramolecular self-assemblies.<sup>2,3</sup> This encoded hierarchical association provides access to ordered nanostructures that are otherwise inaccessible under traditional block-selective solvent processing conditions.<sup>4–13</sup> The amphiphilic balance, physicochemical

properties of the constituent blocks, and processing conditions play a decisive role in the solution-state morphology. In comparison with small-molecule surfactants, the self-assembly behavior of amphiphilic macromolecules is complicated by slow chain dynamics.<sup>14</sup> Consequently, the observed morphologies can be kinetically trapped and far from equilibrium.<sup>15</sup> Since polymeric nanostructures are applied in healthcare and personal care markets, a mechanistic understanding of these morphological transitions is needed.<sup>16–19</sup>

While the specific self-assembled morphology is observable, a mechanistic insight into the transition pathways for a

given polymer composition and processing conditions is challenging.<sup>6,20–27</sup> Analyzing and interpreting co-existing features in an isochronal sample offers insights on morphological transitions. For instance, the pathways from the cylinder to the bilayer or vesicle were documented by accounting for co-existing morphologies in a polydisperse sample.<sup>22,24,27</sup> These examples demonstrate the complexity involved in morphological transitions and the importance of understanding these processes.

Amphiphilic diblock copolymers with hydrophobic side chains display self-assembly through the interplay of micro-phase separation of blocks and packing of the hydrophobic side chains.<sup>28,29</sup> Cholesterol, a vital structural component of animal cell membranes, provides a versatile moiety to direct self-assembly.<sup>30</sup> We have utilized cholesterol either as the side chain or as an initiator for ring opening polymerization to access well-defined materials for biomedical applications.<sup>11,31–38</sup> Aqueous self-assembly of diblock copolymers of poly(ethylene glycol) (PEG) with cholesterol-functionalized aliphatic carbonate (MTC-Chol) blocks, PEG<sub>113</sub>-*b*-P(MTC-Chol)<sub>*n*</sub> forms unique disk-like micelles with *n* = 4 and stacked-disk nanostructures with *n* = 11, where *n* is the MTC-Chol degree of polymerization.<sup>11</sup> Disk-like micelles were formed in other systems under specific processing conditions or with the use of fluoropolymer and/or advanced polymer architectures, such as ABA triblocks with densely grafted middle block or zwitterionic fullerene/polystyrene-based giant surfactants.<sup>39–44</sup> The cholesterol-functionalized polymers find applications in hydrophobic anti-cancer drug sequestration and delivery due to the availability of the cholesterol micelle core. These polymers find use as steric stabilizing additives for hybrid stealth liposomes (HSL) due to the cholesterol end group insertion into the lipid bilayer.<sup>37,38</sup> A critical average number of cholesterol groups (*n* < 4.8) was observed that led to stable HSL. However, more cholesterol groups led to less stable HSL, suggesting a more favorable pathway toward micellization, rather than liposome insertion.

The effect of higher cholesteryl-containing block compositions offers a model system to systematically study pathways to unconventional nanostructures observed in other systems.<sup>45,46</sup> Here, we report multiple pathways to access different nanostructures from a single precursor, PEGylated amphiphilic diblock copolymer **1** [PEG<sub>113</sub>-*b*-P(MTC-Chol)<sub>30</sub>] (Scheme 1). Systematic changes in the solution processing including the choice of organic solvents such as

dimethylformamide, tetrahydrofuran (THF), dioxane, and methanol used to dissolve the polymer lead to pathway-dependent morphologies upon dialysis against water. Characterization of self-assembled morphologies under aqueous conditions by transmission electron microscopy (TEM), cryogenic TEM, and small-angle neutron scattering (SANS) offers insights into the mechanistic pathways. The resultant nanostructures have distinct discrete disks, hierarchical features, or asymmetric growth associated with the sample processing history. These findings highlight how amphiphilic block copolymers with structure-directing groups offer various nanostructures with a limited set of building blocks.<sup>15</sup>

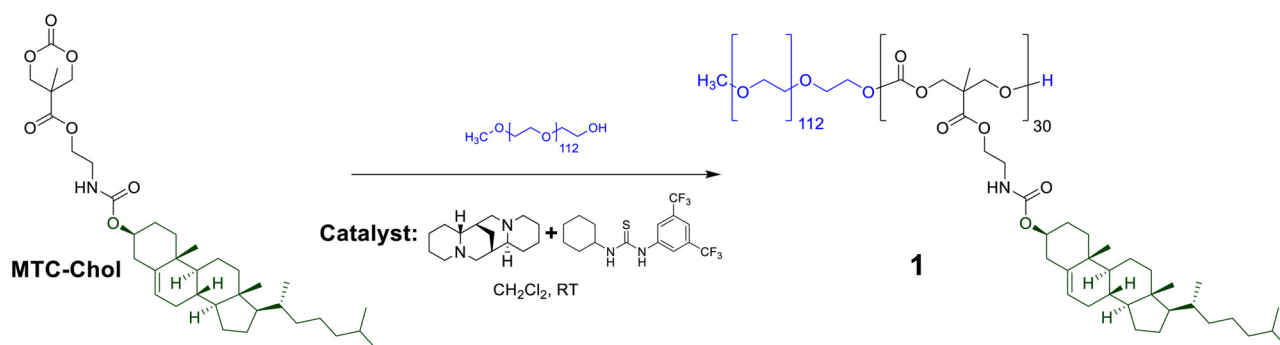
## MATERIALS AND EXPERIMENTAL METHODS

### Block copolymer synthesis

The polymer synthesis was conducted using mPEG-OH (5.0 kDa) as the macro-initiator and (–) sparteine/thiourea as the catalyst combination in dichloromethane at room temperature for 24 h in a glovebox. The crude reaction mixture was purified by dialyzing against tetrahydrofuran (THF) to remove any unreacted monomers and catalyst. The degree of polymerization (*DP*<sub>*n*</sub>) of P(MTC-Chol) block was determined by <sup>1</sup>H NMR spectroscopy by comparing the intensity of protons from PEG regions to that of cholesterol, and the *DP*<sub>*n*</sub> of P(MTC-Chol) was found to be 30 units (*f*<sup>(PEG)</sup> ≈ 21% by mass) [Fig. S1(a) in the [supplementary material](#)]. The size-exclusion chromatography of the purified polymer had a unimodal peak [Fig. S1(b) in the [supplementary material](#)] with a narrow molar mass polydispersity (*D*<sub>M</sub>) of 1.21.

### General conditions for block copolymer self-assembly

In a scintillation vial (20 ml) equipped with a magnetic stir bar, block copolymer **1** and organic solvent (polymer concentration: 1.0 mg/ml) were added and stirred under ambient conditions for a few hours. The resultant solution/dispersion was transferred to a dialysis membrane with a molecular mass cutoff of 1000 Da (Spectra/Por<sup>®</sup>; USA) and dialyzed against de-ionized (DI) water (1 L; at room temperature). The water was changed at the following time points: 3 h, 18 h, and 21 h. The final concentration of the polymer solution/dispersion was ≈ 0.4 mg/ml (assuming no



**SCHEME 1.** Synthesis of amphiphilic diblock copolymer **1** via organo-catalytic ring opening polymerization of MTC-Chol monomer.

polymer loss). These procedures were used for the initial organic solvents of dimethylformamide (DMF), tetrahydrofuran, dioxane, and methanol. American Chemical Society (ACS) grade or high pressure liquid chromatography (HPLC) grade solvents were obtained from J. T. Baker or Fisher Scientific and used as received. For experiments involving thermal treatment, freshly prepared self-assemblies were incubated in tightly capped and Parafilm M<sup>®</sup> sealed vials in an oven at the desired temperature. The samples were then transferred onto TEM grids quickly (<1 min). The sample preparation for SANS was similar with details provided in the [supplementary material](#).

### Electron microscopy

TEM was conducted on an FEI Tecnai G2 F20 operating at an acceleration voltage of 200 keV. Samples for TEM were prepared by first placing 4.0  $\mu\text{L}$  of a self-assembled polymer solution or dispersion onto a formvar-coated copper grid (200 mesh; Ted Pella Inc., USA). After one minute, excess solution was removed (via capillary action) by a wedge of a filter paper. Phosphotungstic acid (2% by mass in de-ionized water; 4.0  $\mu\text{L}$ ), the staining agent, was then placed on the grid. One minute later, again, the excess solution of the staining agent was removed via capillary action with a wedge of a filter paper, and the grid was dried under ambient conditions. For polymers in DMF, the same procedure was used except for the carbon type B 200 mesh copper grid (Ted Pella Inc., USA).

Cryo-transmission electron microscopy was conducted using plasma-exposed EMS C-flat carbon grids (10 s exposure for surface hydrophilicity). A Leica EM GP plunge freezer was used to prepare thin, vitreous ice containing polymer assemblies, which were formulated at  $\approx 2$  mg/ml in  $\text{D}_2\text{O}$  (solutions from SANS experiments were used). Imaging was conducted using an FEI Titan G2 microscope operated at an accelerating voltage of 300 kV. No staining was used to aid in the imaging of samples.

### Small-angle neutron scattering

SANS measurements were performed at the National Institute of Standards and Technology Center for Neutron Research NGB 10 m  $n\text{SOFT}$  beam line with cold neutrons. Three combinations of wavelength ( $\lambda$ ) and sample-to-detector distance  $l$  were used ( $\lambda/l = 12 \text{ \AA}/5.2 \text{ m}$ ,  $5 \text{ \AA}/5.2 \text{ m}$ , and  $5 \text{ \AA}/1.2 \text{ m}$ ). The spread of neutrons ( $\Delta\lambda/\lambda$ ) was 0.11. Hellma quartz cuvettes with a path length of 2.0 mm were used for all measurements carried out at 25 °C. The scattered intensity  $I(Q)$  was measured as a function of the wave vector ( $Q$ ) defined by  $Q = (4\pi/\lambda) \sin(\theta/2)$ , where  $\theta$  is the scattering angle. For the polymer dissolved in deuterated dioxane, the NG7 SANS instrument ( $\lambda/l = 6 \text{ \AA}/4 \text{ m}$  and  $6 \text{ \AA}/1 \text{ m}$ ) was used. Data were placed on an absolute intensity scale via direct beam flux measurement, detector sensitivity and element size, transmission, sample-to-detector distance, and sample scattering volume considerations. Standard data reduction routines and scaling to absolute intensity measurements were applied.<sup>47</sup> The background intensity due to incoherent scattering contributions from protons and solvent scattering was estimated and subtracted using established methods.<sup>48</sup> Uncertainties (error bars) are estimated by one standard deviation of the mean by least-squares minimization of fits to the

SANS data. While error bars are shown, they may be smaller than the symbols used in some cases.

## RESULTS AND DISCUSSION

Systematically varying the solvent quality can tailor the self-assembled morphology.<sup>1,15</sup> For the same polymer, different solvents with similar chemical composition, such as THF vs 1,4-dioxane (dioxane), yield different morphologies.<sup>49,50</sup> The choice of the solvent plays a critical role in the self-assembly pathway. Polymer **1** was first dissolved (or dispersed) in a water-miscible organic solvent, followed by dialysis against DI water to yield aqueous assemblies. The role of the initial solvent to dissolve or disperse the polymer and its implications on the self-assembled morphology is investigated.

### Dimethylformamide forms equilibrium stacked disk morphology

Polymer **1** exists as aggregates in DMF due to poor solubility of the P(MTC-Chol) block. Aggregation of **1** in DMF was confirmed by multiple techniques such as  $^1\text{H}$  NMR spectroscopy through a significant reduction in the relative intensity of the P(MTC-Chol) block in comparison with the PEG block, dynamic light scattering, TEM, and optical transmittance measurements (Figs. S2, S3, S7(a), and Table S1 in the [supplementary material](#)). After exchange of DMF with de-ionized water by dialysis, two distinct morphological features were observed by phosphotungstic acid stained conventional TEM and cryo-TEM (no stain): (1) Stacked-disk-like cylinders with a diameter of  $\approx 20$  nm, occasionally with emergent ellipsoidal-like features (Fig. 1). These cylinders retained the hierarchical lamellar-*within*-cylinder (stacked disks) morphology observed with PEG<sub>113</sub>-*b*-P(MTC-Chol)<sub>11</sub>.<sup>11</sup> (2) Large ellipsoids retaining stripe patterns [Figs. 1(b)–1(d), arrow 1] with a uniform periodicity of  $\approx 5$  nm. Attachment of the cylinders at the end of the ellipsoid or at the side of the ellipsoid can be observed [Figs. 1(b) and 2(c), arrows 2 and 3]. These data suggest that the origin of ellipsoids with DMF as the initial solvent is primarily due to the fusion of the cylinders in a parallel direction across their length.

### Tetrahydrofuran forms disk-like micelles

As will be shown, the morphological outcome for THF as the initial solvent was different from that of using dioxane, methanol, or DMF. Discrete disk-like micelles were observed with THF as the initial solvent [Fig. 2(a)]. The presence of prolate or ellipsoidal structures along with the spherical features indicates that these are disk-like micelles [Fig. 2(a)] with an average diameter of  $18.9 \text{ nm} \pm 3.6 \text{ nm}$  over 100 particles.<sup>11,39,40,42</sup> Disk-like morphology of these micelles was further confirmed by tilting the stage and also by cryo-TEM [Fig. S8 in the [supplementary material](#) and Fig. 2(b)]. An overlap of disks in cryo-TEM shows a change in contrast consistent with disk like morphology.

DMF and THF differ in their relative ability to solvate the P(MTC-Chol) block. This distinction motivated us to question whether the two different mechanistic pathways were primarily decided by the nature of the solvated state of the hydrophobic block. To further probe this line of thought, we explored dioxane

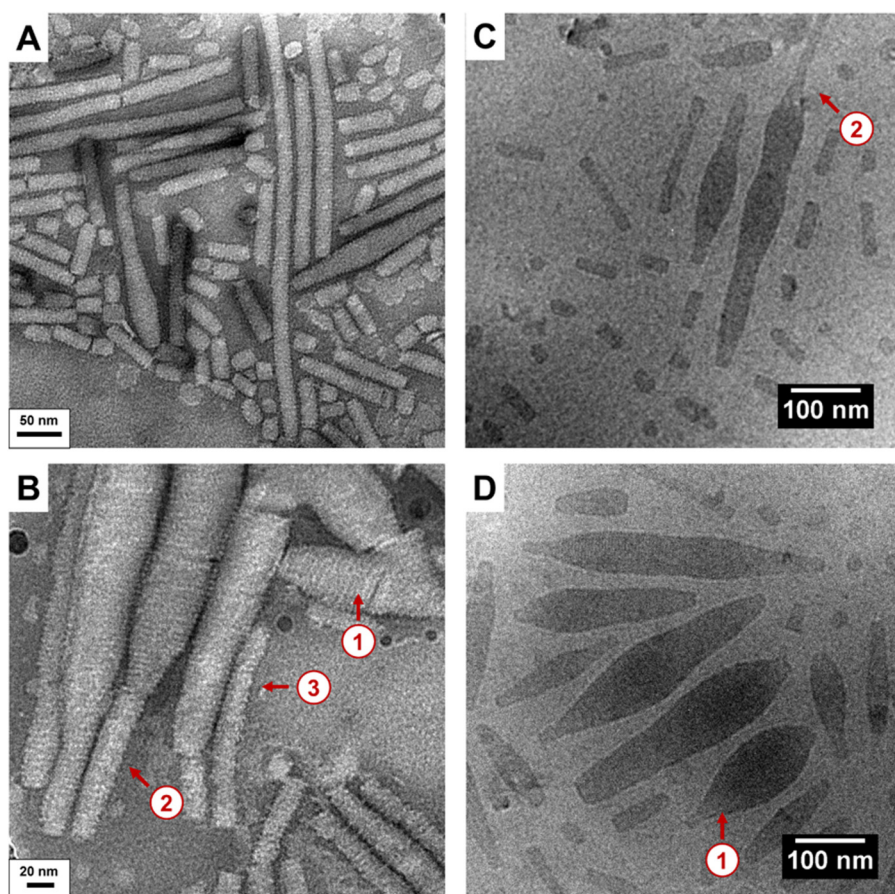


**FIG. 1.** TEM images of the aqueous self-assembly of polymer **1**, prepared via solvent exchange from DMF to DI water observes cylinders (a) and ellipsoids (b) with striped patterns. Both the features have smectic order (labeled by arrow 1) indicative of a stacked-disk structure. Attachment of the cylinders along the end or along the sides of the ellipsoids can be observed (arrows 2 and 3). Cryo-TEM experiments (c) and (d) wherein no staining is employed, and therefore, the contrast is both inverted and weaker. Similar features are observed.

and methanol as another solvent pair. These solvents were chosen by taking note of their relative polarity and ability to dissolve and disperse block copolymer **1**. THF and dioxane are similar in their chemical composition and both served as a good solvent for both

the blocks of polymer **1**. While both methanol and DMF could well suspend polymer **1**, cloudy solutions were observed (Fig. S4 in the [supplementary material](#)) due to their poor ability to solvate the (PMTC-Chol) block.

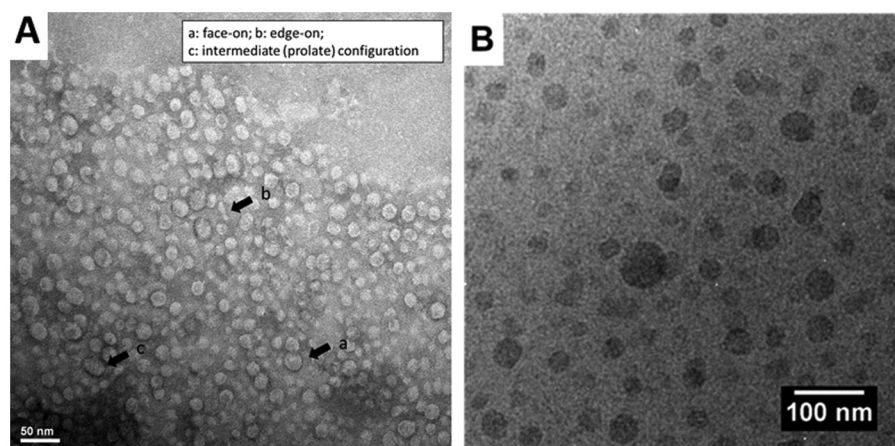


**FIG. 2.** TEM images of the aqueous self-assembly of polymer **1**, prepared via solvent exchange from THF to DI water (the dialysis method). The dialyzed samples had predominantly disk-like micelles (a). Disk-like micelles were also captured using cryo-TEM with no staining employed so that structures appear as inverted and at reduced contrast (b).

### Dioxane forms a stacked disk and asymmetric objects

While THF and dioxane are ethers, the two solvents exhibit distinguishable influence on self-assembly.<sup>49,50</sup> Morphologies accessed from dioxane as the initial organic solvent have four distinct features: (1) *cylinders* of about 12 nm–20 nm diameter and about 20 nm to  $\approx 1 \mu\text{m}$  long (Fig. 3, arrow 1); (2) *bracelets*, consisting of an ellipsoidal feature of about 30 nm–40 nm, flanked by cylinders on both the ends (Fig. 3, arrow 2; a pictorial guide for the morphology related terms used in this paper are provided in the supporting information); (3) *asymmetric multi-tailed objects*, as a variant of the bracelet, with an emerging curvature, ranging from simplest, Y-shaped (Fig. 3, arrow 3) with two-tails to multi-tails with the tails as high as 10 [on the broader side, Figs. 3(e)–3(h)]; and (4) *half-vesicle or bowls* [Fig. 3(a), arrow 4 and 3(i)]. Multi-tailed asymmetric objects, similar to the octopus-like intermediate structures, are observed in other systems involving cylinder-to-vesicle transition,<sup>22,51,52</sup> suggesting that these intermediates are common across mechanistic paths involving fusion of cylinders to higher dimensional aggregates.<sup>20,22,51–54</sup> It is important to note that in our system, we only observed half-vesicles. This could be partly due to the rigidity of these membranes, preventing them from the formation of completely closed structures within the time frame of our experiments. Collectively, these four isochronal features illustrate our hypothesis for the hierarchical association of cylinders.

### Methanol forms stacked disk structures

Similar to DMF, methanol also poorly dissolved polymer 1 as evidenced by the presence of self-assembled aggregate structures in the methanol solution [Fig. S7(b) in the [supplementary material](#)]. After dialysis against water, the morphology was similar to that of DMF, with some branched Y-like cylinders present (Fig. 4, arrow 1) and smectic ordering with period  $\approx 5$  nm. Collectively, these results demonstrate that the associative interactions can be manipulated by tailoring the solution-state processing parameters by aqueous dialysis exchange. Organic solvent-polymer interactions dictate the block copolymer chain conformation, which eventually influences the nature of higher-order hierarchical interactions under aqueous conditions.

### STRUCTURE IN ORGANIC SOLVENTS AND AFTER DEUTERIUM OXIDE DIALYSIS

We used SANS to characterize the structure of polymer 1 before and after dialysis. Before dialysis, a Bragg scattering peak  $Q^*$ , attributed to the cholesterol side-chain ordering, was observed in *d*-DMF [Fig. 5(a)] and in *d*-methanol (Fig. S10 in the [supplementary material](#)). This result suggests that DMF and methanol are poor solvent for the MTC-Chol block; therefore, a self-assembled structure exists even before dialysis against  $\text{D}_2\text{O}$ . In contrast, no Bragg scattering peak  $Q^*$  was observed in *d*-THF

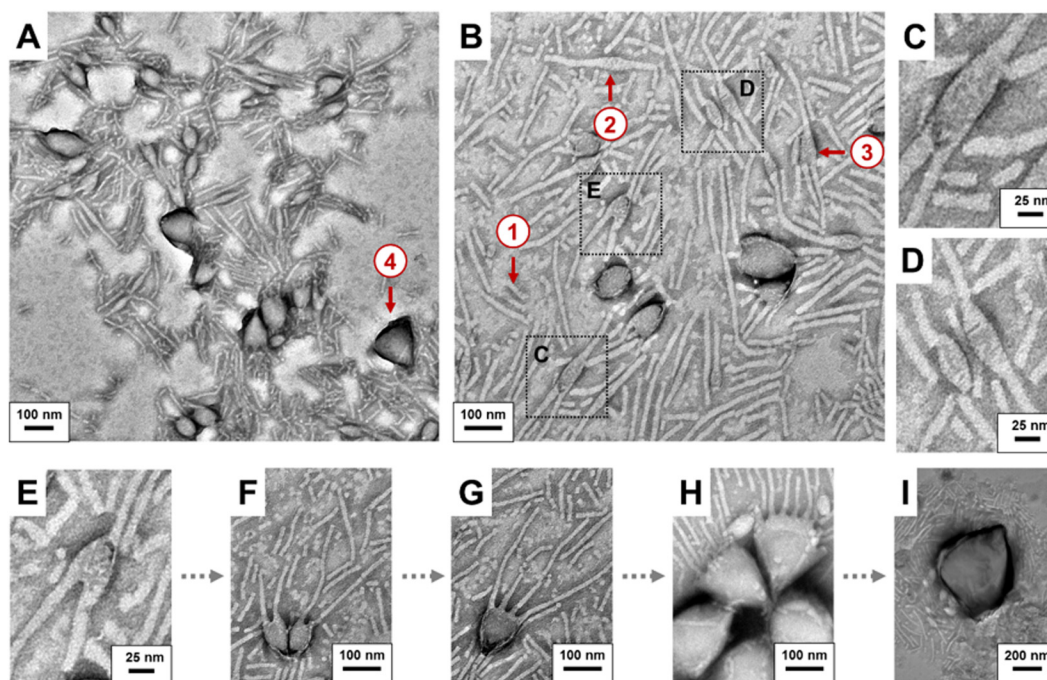


**FIG. 3.** TEM images of the aqueous self-assembly of polymer 1, prepared via solvent exchange from dioxane to DI water via the dialysis method. (a) and (b) are representative micrographs, showing the four major features, corresponding to the hypothetical sequence of morphological transformation cylinders (arrow 1) to bracelets (2), asymmetric multi-tailed objects (3), and half-vesicles (4); (c) Interaction of two cylinders in an “X” fashion with all four “tails” intact and attached to the emergent ellipsoidal feature; (d) Ellipsoid with only two of the cylindrical flanks to form a bracelet (e) “Y”-shaped simplest asymmetric multi-tailed object; (f)–(h) Examples of complex asymmetric multi-tailed objects; and (i) half-vesicle.

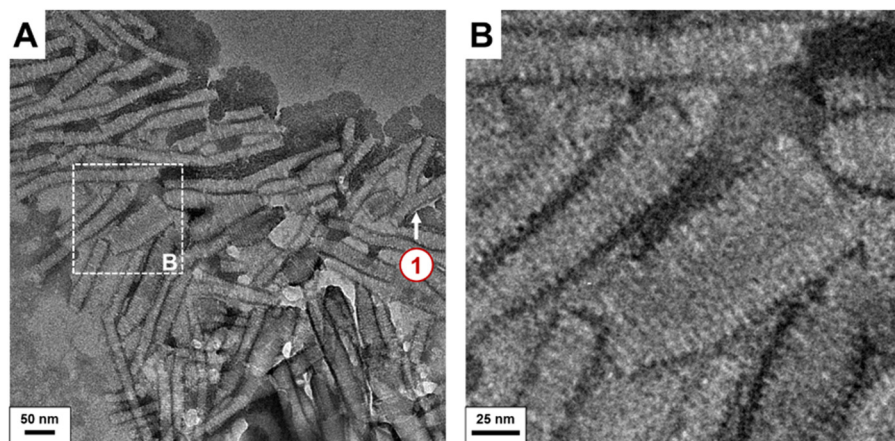


**FIG. 4.** TEM images of the aqueous self-assembly of polymer **1**, prepared via solvent exchange from methanol to DI water (the dialysis method). The dialyzed samples had a (a) mixture of cylinders, Y-junctions (arrow **1**), and other nanostructures with smectic order (b).

[Fig. 5(b)] and *d*-dioxane (Fig. S10 in the supplementary material), indicating that polymer **1** is molecularly dissolved. After dialysis against  $D_2O$ , the Bragg scattering peak  $Q^*$  appears (Fig. 5). We observed that the peak width of  $Q^*$  dialyzed from *d*-DMF [Fig. 5(a)] is sharper than the one dialyzed from *d*-THF [Fig. 5(b)]. The sharper peak indicates a more ordered self-assembled structure. SANS data also show that thermal annealing has no significant effect on self-assembled structures.

A summary of the structural parameters obtained with SANS is shown in Table I. The smectic order period due to ordered cholesteryl side chains, calculated as  $d = 2\pi/Q^*$ , is about 5 nm. For the self-assembled structure of cylinders, we estimated the cross-sectional radius of gyration ( $R_{g,c}$ ) with a Guinier-like limiting law where the form of the scattering follows  $I \times Q \approx \exp\left(\frac{-Q^2 R_{g,c}^2}{2}\right)$ .<sup>11</sup> On a plot of  $\ln(IQ)$  vs  $Q^2$ , the slope provides a  $R_{g,c}$  value (Figs. S12 and S13 in the supplementary material). The average

diameter of the cylinder ( $D$ ) is estimated as  $D = 2\sqrt{2}R_{g,c}$ . Cylinders dialyzed from DMF show a larger structure (larger  $R_{g,c}$  and  $D$ ) than the ones dialyzed from dioxane (Table I). Unlike DMF and dioxane, disk-like micelles were formed when dialyzed from THF. In this case, radius of gyration ( $R_g$ ) along the disk thickness (4 nm–5 nm) was estimated from the plot of  $\ln(IQ^2)$  vs  $Q^2$  (Fig. S14 in the supplementary material).<sup>55</sup> No changes were observed in the structure parameters after annealing the post-dialyzed aqueous solution at 65 °C for 16 h, indicating that MTC-Chol blocks are kinetically trapped because of the high association energy of MTC-Chol in water.<sup>56</sup>

TEM and SANS data show that the self-assembly of polymer **1** is pathway dependent. The structure of polymer **1** after dialysis against water depends on the initial organic solvent quality. We estimated the solubility parameters ( $\delta_t$ ) to characterize the relative quality of a specific solvent. As shown in Table II,  $\delta_t$  was calculated by the method of Hoftyzer and Van Krevelen,<sup>57</sup> and the calculated

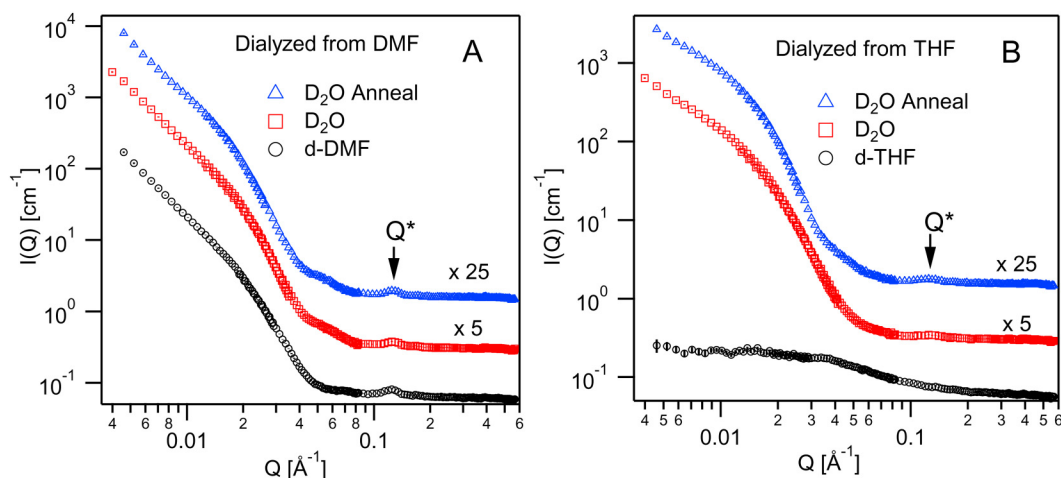


**FIG. 5.** SANS patterns of polymer **1** in deuterated organic solvents, in  $D_2O$  via the dialysis method, and in  $D_2O$  via the dialysis method after annealed for 16 h at 65 °C, respectively. (a) DMF as the initial organic solvent. (b) THF as the initial organic solvent. The patterns are shifted vertically for clarity. A scattering peak was identified,  $Q^*$ .

**TABLE I.** Size and shape characteristics of polymer 1 in different solvents. Uncertainties (error bars) are estimated by one standard deviation of the mean by least-squares minimization of fits to the SANS data.

	Hierarchical cylinder structure			Disk structure $R_g$ along disk thickness (nm)
	Smectic order period, $d$ (nm)	Cross section $R_{g,c}$ (nm)	Diameter, $D = 2\sqrt{2}R_{g,c}$ (nm)	
<i>d</i> -THF <sup>a</sup>				
D <sub>2</sub> O(THF)	4.90 ± 0.08			4.49 ± 0.01
D <sub>2</sub> O(THF) anneal	5.03 ± 0.05			5.67 ± 0.02
<i>d</i> -dioxane <sup>b</sup>				
D <sub>2</sub> O(dioxane)	4.91 ± 0.03	9.5 ± 0.3	26.9 ± 0.8	
D <sub>2</sub> O(dioxane) anneal	4.92 ± 0.02	10.0 ± 0.3	28.4 ± 0.7	
<i>d</i> -DMF	5.05 ± 0.02	12.5 ± 0.2	35.3 ± 0.7	
D <sub>2</sub> O(DMF)	4.97 ± 0.02	12.3 ± 0.2	34.8 ± 0.6	
D <sub>2</sub> O(DMF) anneal	4.95 ± 0.02	11.8 ± 0.2	33.4 ± 0.6	
<i>d</i> -methanol	4.80 ± 0.2			

<sup>a</sup>(3.35 ± 0.02) nm dissolved chain radius of gyration estimated by the Debye chain form factor.

<sup>b</sup>(3.30 ± 0.03) nm dissolved chain radius of gyration estimated by the Debye chain form factor.

values agree well with the literature values.<sup>58</sup> According to like-dissolves-like, the rank of solvent quality for MTC-Chol block is THF > dioxane > DMF > methanol > H<sub>2</sub>O where THF is a good solvent, while H<sub>2</sub>O is a poor solvent. Table S4 in the [supplementary material](#) provides further details on the polar, dispersive, and hydrogen bonding contributions to the total solubility parameter.

The solvent-quality rank is consistent with the results obtained from SANS and TEM. SANS shows that no peak Q\* is observed in *d*-THF [Fig. 5(b) and Table I] and polymer 1 is molecularly dissolved, which agrees with the results suggested by  $\delta_t$  that THF is a good solvent for a MTC-Chol block (Table II). In this case, dialysis leads to primarily discrete disk-like micelles (Fig. 2). Similar to THF, polymer 1 is molecularly dissolved in *d*-dioxane (Fig. S10 in the [supplementary material](#) and Table I). But because dioxane has a lower solvent quality for the MTC-Chol block than THF (Table II), the driving force to sequester is larger and leads to the stacked cylinder with an asymmetric structure after dialysis (Fig. 3).

Unlike THF and dioxane, self-assembly takes place in DMF and methanol as shown by SANS [Figs. 5(a) and S10 in the [supplementary material](#) and Table I]. Correspondingly,  $\delta_t$  values indicate that solvent quality of DMF and methanol is much poorer than THF and dioxane for the MTC-Chol block (Table II). Therefore, even in organic solvent, ordered packing of cholesterol side

chains exists and dialysis exchange to water preserves the structure. The larger mismatch in solute-solvent quality appears to further drive the discrete disk-like micelle into the stacked-disk-like cylinders further sequestering the MTC-Chol segments (Figs. 1 and 4). We noticed that the smectic order period ( $d \approx 5$  nm) calculated from peak Q\* exists in all aqueous solutions and in organic solvents of DMF and methanol (Table I). This result indicates that ordered packing of cholesterol side chains may serve as a precursor structure for the pathway-dependent nanostructures via an aqueous self-assembly. Taken together, we suggest that aqueous self-assembled structure of polymer 1 dialyzed from organic solvent becomes mature, i.e., developing from discrete disk-like micelle (induced from THF) to a stacked-disk-like cylinder (induced from dioxane) and to a more ordered hierarchical structure (induced from DMF and methanol), when the organic solvent quality decreases gradually.

## CONCLUSIONS

A single polymer precursor based on cholesterol-functionalized aliphatic polycarbonate-based amphiphilic diblock copolymer, (PEG<sub>113</sub>-*b*-P(MTC-Chol)<sub>30</sub>) (1) provides access to pathway-dependent nanostructures via aqueous self-assembly. The initial organic solvent that dissolves or disperses the polymer dictates the pathway to nanostructures with distinguishing features such as discrete disks, stacked disks, and asymmetric growth or hierarchical features. Observation of self-assembled morphologies by TEM and structural details extracted from SANS offered insights into different mechanistic pathways. The process of organic solvent dissolution followed by dialysis may lead to structures that are far from equilibrium. Nevertheless, a correlation between solubility parameter and pathway-dependent morphology was observed. The organic solvent that is poorest for the MTC-Chol block drives the self-assembly leading to hierarchical structures. Whereas the best solvent with lowest  $\delta_t$  induces primarily disks, as demonstrated with THF. Accessing these distinct hierarchical nanostructures and understanding of their self-assembly behaviors can provide

**TABLE II.** Solubility parameters  $\delta_t$  estimated by the method of Hoftyzer and Van Krevelen.

Polymers and solvents	$\delta_t$ (J <sup>1/2</sup> cm <sup>-3/2</sup> )
PEO	22.0
P(MTC-Chol)	14.1
THF	19.4
Dioxane	20.5
DMF	24.9
Methanol	29.6
H <sub>2</sub> O	47.9

templates for the synthesis of nanostructured composite materials and preferential loading of cargo, such as hydrophobic drugs. The process conditions and structure observed are not general and will depend upon the polymer composition and molecular mass.

## SUPPLEMENTARY MATERIAL

See the [supplementary material](#) for additional details on materials and methods, synthesis of polymer **I**, self-assembly conditions, <sup>1</sup>H NMR and SEC, photos of polymer **I** in different solvents, TEM, tilt-study TEM, and cryo-TEM, SANS data and curve fitting, and solubility parameter calculations.

## ACKNOWLEDGMENTS

S.V., J.L.H., and Y.Y.Y. acknowledge funding by the Institute of Bioengineering and Nanotechnology (Biomedical Research Council, Agency for Science, Technology and Research, Singapore) and IBM Almaden Research Center. V.M.P., K.P.M., and G.W. thank the support of the National Institute of Standards and Technology (NIST) Materials Genome Initiative and R.L. Jones, Director of the nSOFT beam line at the NIST Center for Neutron Research. K.P.M. acknowledges the NIST National Research Council Research Associateship Program.

Certain commercial equipment and materials are identified in this paper in order to specify adequately the experimental procedure. In no case does such identification imply recommendations by the National Institute of Standards and Technology (NIST) nor does it imply that the material or equipment identified is necessarily the best available for this purpose.

## REFERENCES

- <sup>1</sup>Y. Mai and A. Eisenberg, *Chem. Soc. Rev.* **41**, 5969 (2012).
- <sup>2</sup>O. Ikkala and G. ten Brinke, *Chem. Commun.* **19**, 2131 (2004).
- <sup>3</sup>A. Wang, J. Huang, and Y. Yan, *Soft Matter* **10**, 3362 (2014).
- <sup>4</sup>H. Qiu, Z. M. Hudson, M. A. Winnik, and I. Manners, *Science* **347**, 1329 (2015).
- <sup>5</sup>Z. Li, E. Kesselman, Y. Talmon, M. A. Hillmyer, and T. P. Lodge, *Science* **306**, 98 (2004).
- <sup>6</sup>J. Zhu and W. Jiang, *Macromolecules* **38**, 9315 (2005).
- <sup>7</sup>H. Cui, Z. Chen, S. Zhong, K. L. Wooley, and D. J. Pochan, *Science* **317**, 647 (2007).
- <sup>8</sup>E. Lee, B. Hammer, J.-K. Kim, Z. Page, T. Emrick, and R. C. Hayward, *J. Am. Chem. Soc.* **133**, 10390 (2011).
- <sup>9</sup>A. J. Soininen, A. Rahikkala, J. T. Korhonen, E. I. Kauppinen, R. Mezzenga, J. Raula, and J. Ruokolainen, *Macromolecules* **45**, 8743 (2012).
- <sup>10</sup>A. H. Gröschel, F. H. Schacher, H. Schmalz, O. V. Borisov, E. B. Zhulina, A. Walther, and A. H. E. Müller, *Nat. Commun.* **3**, 710 (2012).
- <sup>11</sup>S. Venkataraman, A. L. Lee, H. T. Maune, J. L. Hedrick, V. M. Prabhu, and Y. Y. Yang, *Macromolecules* **46**, 4839 (2013).
- <sup>12</sup>X. Chen, W. Wang, S. Cheng, B. Dong, and C. Y. Li, *ACS Nano* **7**, 8251 (2013).
- <sup>13</sup>T. I. Löbbling, O. Borisov, J. S. Haataja, O. Ikkala, A. H. Gröschel, and A. H. E. Müller, *Nat. Commun.* **7**, 12097 (2016).
- <sup>14</sup>A. Halperin, *J. Macromol. Sci. Part C: Polym. Rev.* **46**, 173 (2006).
- <sup>15</sup>R. C. Hayward and D. J. Pochan, *Macromolecules* **43**, 3577 (2010).
- <sup>16</sup>C. K. Ober, S. Z. D. Cheng, P. T. Hammond, M. Muthukumar, E. Reichmanis, K. L. Wooley, and T. P. Lodge, *Macromolecules* **42**, 465 (2009).
- <sup>17</sup>A. Blanz, S. P. Armes, and A. J. Ryan, *Macromol. Rapid Commun.* **30**, 267 (2009).
- <sup>18</sup>S. Venkataraman, J. L. Hedrick, Z. Y. Ong, C. Yang, P. L. R. Ee, P. T. Hammond, and Y. Y. Yang, *Adv. Drug Delivery Rev.* **63**, 1228 (2011).
- <sup>19</sup>Y. Wang, J. He, C. Liu, W. H. Chong, and H. Chen, *Angew. Chem. Int. Ed.* **54**, 2022 (2015).
- <sup>20</sup>C. Fernyhough, A. J. Ryan, and G. Battaglia, *Soft Matter* **5**, 1674 (2009).
- <sup>21</sup>A. G. Denkova, E. Mendes, and M.-O. Coppens, *Soft Matter* **6**, 2351 (2010).
- <sup>22</sup>A. Blanz, J. Madsen, G. Battaglia, A. J. Ryan, and S. P. Armes, *J. Am. Chem. Soc.* **133**, 16581 (2011).
- <sup>23</sup>D. Han, X. Li, S. Hong, H. Jinnai, and G. Liu, *Soft Matter* **8**, 2144 (2012).
- <sup>24</sup>C. Liu, L. Yao, H. Wang, Z. R. Phua, X. Song, and H. Chen, *Small* **10**, 1332 (2014).
- <sup>25</sup>G. Rizis, T. G. M. van de Ven, and A. Eisenberg, *Soft Matter* **10**, 2825 (2014).
- <sup>26</sup>L. Wang, H. Huang, and T. He, *ACS Macro Lett.* **3**, 433 (2014).
- <sup>27</sup>G. Rizis, T. G. M. van de Ven, and A. Eisenberg, *Angew. Chem. Int. Ed.* **53**, 9000 (2014).
- <sup>28</sup>B. Olsen and R. Segalman, *Mater. Sci. Eng.: R: Rep.* **62**, 37 (2008).
- <sup>29</sup>T. Ganicz and W. Stańczyk, *Materials* **2**, 95 (2009).
- <sup>30</sup>Y. Zhou, V. Briand, N. Sharma, S. Ahn, and R. Kasi, *Materials* **2**, 636 (2009).
- <sup>31</sup>D. Zhang, P. D. Hamilton, J. L.-F. Kao, S. Venkataraman, K. L. Wooley, and N. Ravi, *J. Polym. Sci. Part A: Polym. Chem.* **45**, 2569 (2007).
- <sup>32</sup>A. L. Z. Lee, S. Venkataraman, S. B. M. Sirat, S. Gao, J. L. Hedrick, and Y. Y. Yang, *Biomaterials* **33**, 1921 (2012).
- <sup>33</sup>S. Venkataraman, N. Veronica, Z. X. Voo, J. L. Hedrick, and Y. Y. Yang, *Polym. Chem.* **4**, 2945 (2013).
- <sup>34</sup>D. J. Coady, Z. Y. Ong, P. S. Lee, S. Venkataraman, W. Chin, A. C. Engler, Y. Y. Yang, and J. L. Hedrick, *Adv. Healthcare Mater.* **3**, 882 (2014).
- <sup>35</sup>A. L. Z. Lee, S. Venkataraman, C. H. Fox, D. J. Coady, C. W. Frank, J. L. Hedrick, and Y. Y. Yang, *J. Mater. Chem. B* **3**, 6953 (2015).
- <sup>36</sup>C. Yang, S. Q. Liu, S. Venkataraman, S. J. Gao, X. Ke, X. T. Chia, J. L. Hedrick, and Y. Y. Yang, *J. Controlled Release* **208**, 93 (2015).
- <sup>37</sup>S. Venkataraman, K. P. Mineart, V. M. Prabhu, J. L. Hedrick, and Y. Y. Yang, *Polym. Chem.* **9**, 2434 (2018).
- <sup>38</sup>K. P. Mineart, S. Venkataraman, Y. Y. Yang, J. L. Hedrick, and V. M. Prabhu, *Macromolecules* **51**, 3184 (2018).
- <sup>39</sup>Z. Li, Z. Chen, H. Cui, K. Hales, K. Qi, K. L. Wooley, and D. J. Pochan, *Langmuir* **21**, 7533 (2005).
- <sup>40</sup>W. F. Edmonds, Z. Li, M. A. Hillmyer, and T. P. Lodge, *Macromolecules* **39**, 4526 (2006).
- <sup>41</sup>L. Yin and M. A. Hillmyer, *Macromolecules* **44**, 3021 (2011).
- <sup>42</sup>S. J. Holder and N. A. J. M. Sommerdijk, *Polym. Chem.* **2**, 1018 (2011).
- <sup>43</sup>Y. Shi, W. Zhu, D. Yao, M. Long, B. Peng, K. Zhang, and Y. Chen, *ACS Macro Lett.* **3**, 70 (2014).
- <sup>44</sup>Z. Lin, J. Sun, Y. Zhou, Y. Wang, H. Xu, X. Yang, H. Su, H. Cui, T. Aida, W. Zhang, and S. Z. D. Cheng, *J. Am. Chem. Soc.* **139**, 5883 (2017).
- <sup>45</sup>R. Piñol, L. Jia, F. Gubellini, D. Lévy, P.-A. Albouy, P. Keller, A. Cao, and M.-H. Li, *Macromolecules* **40**, 5625 (2007).
- <sup>46</sup>L. Zhou, D. Zhang, S. Hocine, A. Pilone, S. Trépout, S. Marco, C. Thomas, J. Guo, and M.-H. Li, *Polym. Chem.* **8**, 4776 (2017).
- <sup>47</sup>S. R. Kline, *J. Appl. Crystallogr.* **39**, 895 (2006).
- <sup>48</sup>H. Hayashi, P. J. Flory, and G. D. Wignall, *Macromolecules* **16**, 1328 (1983).
- <sup>49</sup>Y. Yu and A. Eisenberg, *J. Am. Chem. Soc.* **119**, 8383 (1997).
- <sup>50</sup>L. Jia, P.-A. Albouy, A. Di Cicco, A. Cao, and M.-H. Li, *Polymer* **52**, 2565 (2011).
- <sup>51</sup>S. Jain and F. S. Bates, *Macromolecules* **37**, 1511 (2004).
- <sup>52</sup>Z. Li, M. A. Hillmyer, and T. P. Lodge, *Nano Lett.* **6**, 1245 (2006).
- <sup>53</sup>A. Rank, S. Hauschild, S. Förster, and R. Schubert, *Langmuir* **25**, 1337 (2009).
- <sup>54</sup>H. Noguchi, *Soft Matter* **8**, 8926 (2012).
- <sup>55</sup>O. Glatter and O. Kratky, *Small Angle X-Ray Scattering* (Academic Press, 1982).
- <sup>56</sup>F. Tanaka and S. F. Edwards, *Macromolecules* **25**, 1516 (1992).
- <sup>57</sup>D. W. Van Krevelen and K. Te Nijenhuis, *Properties of Polymers: Their Correlation with Chemical Structure; Their Numerical Estimation and Prediction From Additive Group Contributions* (Elsevier, 2009).
- <sup>58</sup>A. F. M. Barton, *Chem. Rev.* **75**, 731 (1975).